JOURNAL OF PROPULSION AND POWER
Vol. 24, No. 5, September–October 2008

Flow Study of a Redesigned High-Pressure-Ratio Centrifugal Compressor

H. Krain* and B. Hoffmann*
DLR, German Aerospace Center, 51147 Cologne, Germany

DOI: 10.2514/1.35559

A high-specific-speed, 6:1 total pressure ratio, centrifugal compressor rotor has been improved by using knowledge gained from previous investigations on similar types of compressors as well as advanced three-dimensional design calculations. The new rotor has the same main dimensions as its predecessor and was designed for the same operating point. It was tested with conventional and optical measurement techniques. Performance and optical measurements were carried out up to tip speeds of 586 m/s. The corresponding blade path frequency was 21 kHz. The investigations were supported by three-dimensional stage calculations that delivered detailed insight into the impeller and diffuser flow development. For the high-pressure region, the investigations confirmed an improved compressor performance obtained by the combined experimental/theoretical approach. The enhanced performance can be distinctly attributed to the new impeller concept.

Nomenclature

c	=	absolute velocity, m/s
$D1$	=	vaned diffuser
Eta	=	isentropic stage efficiency
M	=	Mach number
m	=	mass flow rate
n	=	shaft speed, 1/ min
P	=	pressure, N/m^2
Pi	=	pressure ratio
r	=	radius
red	=	corrected
rel	=	relative
st	=	static
sts	=	isentropic, static/total
stt	=	isentropic, total/total
t	=	total
u	=	circumferential speed, m/s
1, 2	=	rotor inlet/rotor exit
$1t$	=	rotor-tip leading edge
3, 4	=	diffuser inlet/diffuser exit

I. Introduction

CENTRIFUGAL compressors are used in many technical fields, for instance, in small gas turbines, turbochargers, process and chemical engineering, aviation, etc. In most fields of application there are strong requirements for compact machines with high power densities, because this generally results in manufacturing cost and weight savings.

It is well known that flow separation very often appears inside high-pressure-ratio centrifugal compressor rotors, resulting in significant inhomogeneous rotor exit flow [1–6]. The unfavorable rotor exit flow conditions generally express themselves in considerable unsteady flow in the absolute frame and in high flow-angle differences between hub and shroud close to the rotor discharge. The disturbed flow impinges on the vaned diffuser, causing a significant incidence distribution across the vaned diffuser height. In the compressors investigated, the flow situation described was caused by a distinct flow separation at the hub close to the rotor leading edge and the development of a wake flow along the shroud. The flow separation close to the rotor inlet was initiated by the radially oriented rotor blade leading edges. The wake flow was caused by the strong curvature at the shroud and by the flow swirl inside the rotor. In principle, the strong shroud curvature is unavoidable for very compact centrifugal rotors but can be designed in different ways. Therefore, it was assumed that an improvement of rotor and diffuser flow can be obtained by achieving a more homogeneous/regular rotor exit flow. To reach this target, new rotor blades had to be designed to suppress the development of separation and wake flow inside the flow channels. Similar to the design of axial machines, an additional positive influence on the 3-D flowfield was expected by a redesign of the meridional contour, which was expected to result in improved rotor-tip clearance and secondary flow.

Received 8 November 2007; revision received 17 March 2008; accepted for publication 18 March 2008.

*Research Engineer, Linder Höhe.

II. Test Compressor and Measurement Technique

Following the described idea, a new high-pressure-ratio, high-specific-speed, transonic centrifugal compressor rotor was designed, manufactured, and tested with advanced techniques, including laser measurements inside the rotating system [7,8]. Figure 1 shows photographs of both the predecessor and the new rotor, each having 13 main and 13 splitter blades.

The main dimensions such as rotor exit radii, lengths, and inlet diameters are identical. Significant differences in blade geometry are obvious at the main blade leading edges and at the impeller exit. Because of stress considerations, radially oriented leading edges were used for the old impeller, whereas the new rotor has swept and backward-leaning blade leading edges. Figure 1 also shows a solid of the centrifugal compressor stage under consideration. The stage is installed in a casing with two exchangeable covers. One is especially designed for detailed acoustic and optical flow measurements. The other cover has a series of holes for static and total pressure measurements as well as tip clearance control and was used for performance evaluation.

The specifications for the centrifugal compressor test facility are listed in Table 1. The most advantageous features are the relatively high rotor-tip speed and the maximum power input, which enables testing high-pressure-ratio transonic centrifugal compressors under realistic operating conditions.

For performance analysis, mass flow and shaft speed, total pressures, and total temperatures at the inlet and exit of the stage were recorded. Additionally, a series of static pressure taps was inserted into the cover for measuring the pressure rise throughout the stage, from rotor inlet to diffuser exit. Furthermore, a number of taps were installed circumferentially at the rotor and diffuser exits to derive

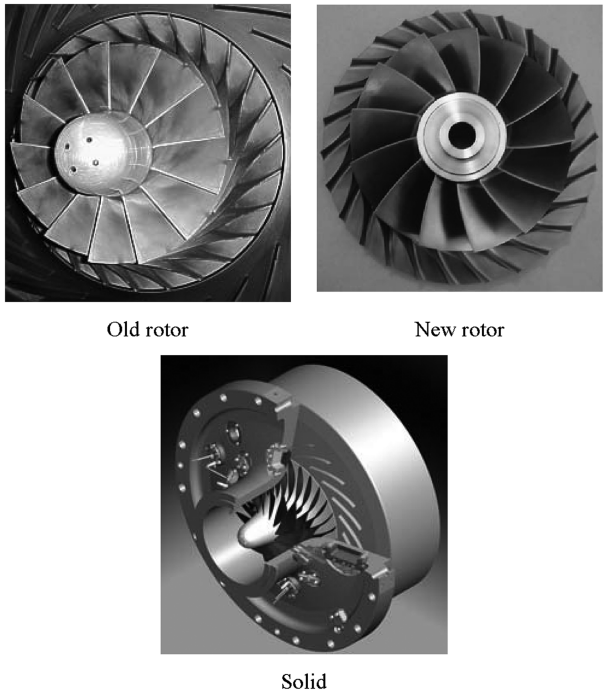

Fig. 1 Photographs of old and new rotors and a solid of the centrifugal compressor stage and casing with windows for optical measurements.

mean static pressures at these positions, needed for deriving rotor efficiency and diffuser recovery. The accuracy in mass flow and shaft-speed measurement was estimated to be better than 0.5%.

For optical measurements inside the rotating system, the well-known laser-two-focus system (L2F) was used at the exit of the rotor, where channel heights are small and where the flow was expected to be almost 2-D and perpendicular to the laser beam axis [7]. Further upstream, the 3-component Doppler-L2F system was used, which combines the principles of the L2F measurement technique and the Doppler global velocimetry [8]. The two absolute-velocity components perpendicular to the laser beam are measured by the L2F principle, and the third component parallel to the laser beam is analyzed by the Doppler principle. The system was especially developed for optical measurements in compact turbomachines. A 1% accuracy in absolute-velocity measurement and 1-deg accuracy in flow angle can be assumed.

In Fig. 2, the 3-component system is shown operating in the test facility. The optical head is rather small and built like a probe to ensure measurements in a narrow environment.

III. Compressor Design and Performance

The transonic rotor was designed by applying the knowledge gained from previous experimental and theoretical investigations on similar types of compressors [1–4]. The main deficits found were extenuated by modifying the blade and meridional geometry. Twenty-two steps were necessary to find a theoretically satisfactory solution. The step-to-step progress was evaluated by the stationary 3-D computational fluid dynamics (CFD) results obtained for each

Table 1 Test-rig specifications

Maximum power input	1500 kW
Maximum shaft speed	60,000 1/min
Maximum rotor-tip speed	700 m/s
Maximum pressure ratio	9.5:1
Maximum flow rate	3.5 kg/s
Maximum rotor-tip diameter	250 mm
Tip diameter test rotor	224 mm
Maximum stage diameter	600 mm
Powered by	Two dc motors

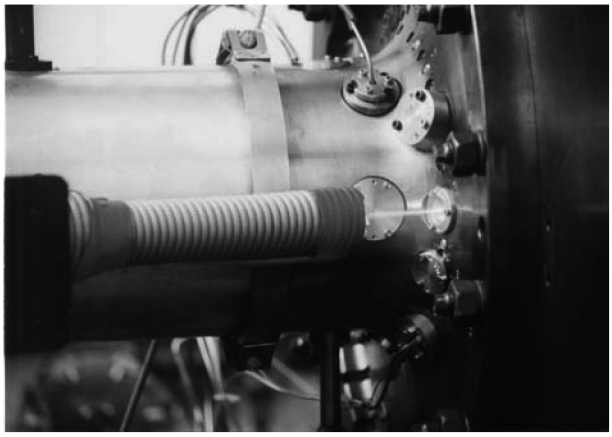

Fig. 2 3C-Doppler-L2F probe operating on the high-speed compressor.

design with the commercial software CFX [9,10], which was available from several companies participating in the research project. The performance characteristics predicted at design speed and the theoretical standard deviation of the flow pattern from block flow at the rotor exit were the main design criteria. To ensure time-saving and low-cost manufacturing on 5-axis milling machines, the blade surfaces of both the main and splitter blade were generated by ruled lines.

The measured compressor performance map is shown in Fig. 3. During these measurements, the rotor SRV4 was coupled with the vaned diffuser shown in the lower part of Fig. 1. Static/total stage pressure ratios versus corrected mass flow rate are plotted with shaft speed as the parameter.

Additionally, contour lines of the measured static/total isentropic stage efficiency are plotted. The maximum pressure ratio achieved is 5.43:1 and maximum efficiency is 79%. The corresponding total/total values are $Pi_{tt\max} = 5.8{:}1$ and $Eta_{stt\max} = 84\%$ respectively. Although the performance map of Fig. 3 assumes that the kinetic energy present at the diffuser exit is completely lost, which is the most unfavorable case from an energetic point of view, a maximum efficiency of 79% can be achieved. The kink in the surge line at 44,000 1/min has not yet been clarified. Surge was detected acoustically. Detailed investigations at slightly higher and lower shaft speeds indicated that a safe compressor operation seems to be possible at mass flow rates lower than those shown in the performance map. However, for safety reasons, long-duration investigations were only carried out at the operating points indicated in Fig. 3.

The total/total values describe the most favorable case in which the remaining kinetic energy at the diffuser exit is decelerated without

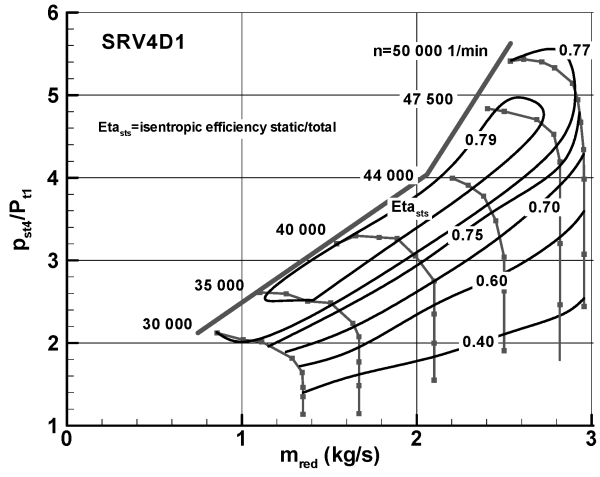

Fig. 3 Performance map of new centrifugal compressor stage SRV4D1.

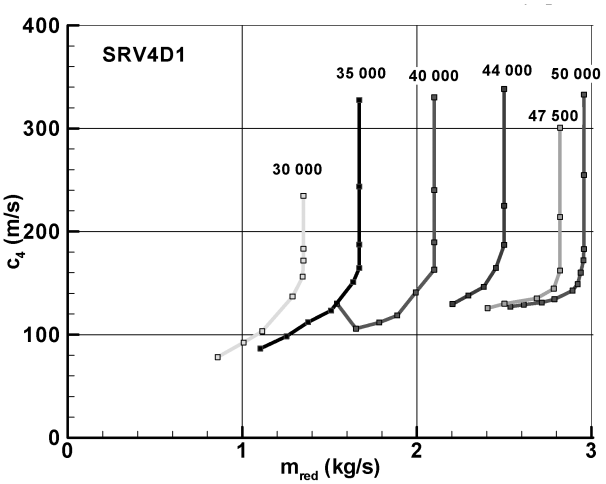

Fig. 4 Absolute velocity at diffuser exit $r/r_2 = 1.9$.

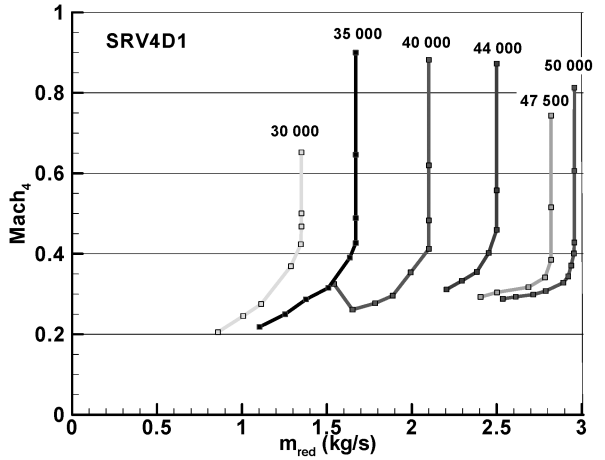

Fig. 5 Absolute Mach number at diffuser exit $r/r_2 = 1.9$.

losses to zero velocity. In reality, an efficiency and a pressure ratio between these extreme values will result if a scroll or exit guide vane is used after the diffuser.

The still-available kinetic energy at the diffuser exit is plotted in Figs. 4 and 5, showing the absolute velocity and absolute Mach number derived from the measurements. The absolute Mach number at the diffuser exit is rather small over the entire operating regime, except at the choke, but due to the high exit temperature, the absolute velocity is still above 100 m/s. Parts of this kinetic energy can be

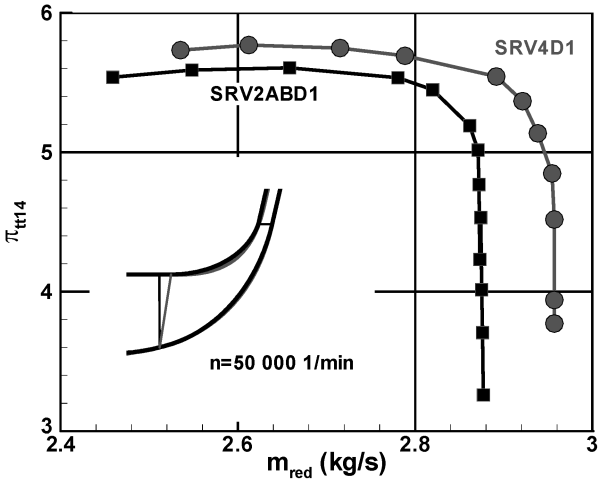

Fig. 6 Comparison of total/total pressure ratio for the old and new designs.

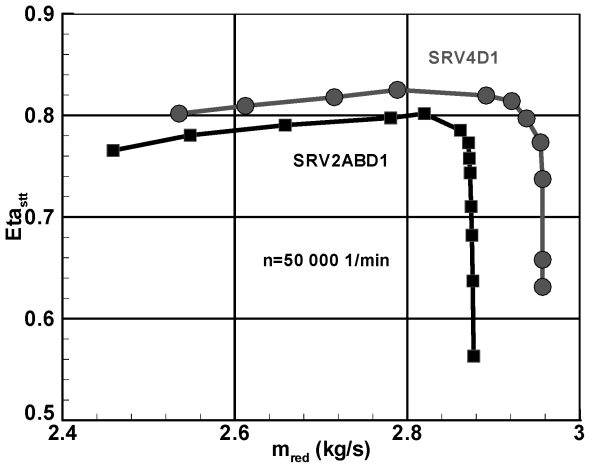

Fig. 7 Comparison of total/total isentropic efficiency for the old and new designs.

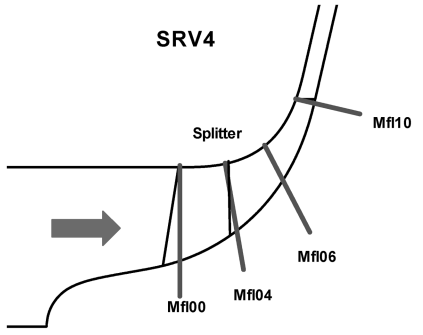

Fig. 8 Location of laser measurement planes in the rotor area.

transferred into additional static pressure rise. The gain in total pressure ratio and total/total isentropic efficiency at design speed for the redesigned rotor in comparison with the predecessor rotor is illustrated in Figs. 6 and 7. The rotors had different meridional cross sections (Fig. 6) and were both coupled with the same diffuser (D1). The total pressure ratio rose by 0.2 bar and the corresponding increase in efficiency was 2% (from 80 to 82%). Because the diffuser was not optimized for the new rotor, the realized gain in performance can be attributed mostly to the improved rotor. This was confirmed by optical flow measurements as well as 3-D flow calculations.

IV. Laser Measurements and Theoretical Analysis

For the analysis of the flow inside the rotating system, laser measurements were performed. The main goal of these measurements was to compare the flow homogeneity before and after redesign.

In Fig. 8, the locations of the laser measurement planes inside the rotor are indicated. They are placed at the same relative meridional positions as for the predecessor rotor SRV2AB (Fig. 1) (i.e., at 0, 40, 60, and 100% meridional flowpath length), starting at the tip leading edge of the full rotor blade. Because the new rotor has backward-leaning leading edges, the meridional shroud length is smaller than that of the old rotor SRV2AB. During the laser measurements, the new rotor was coupled with the vaned diffuser.

Measurements were carried out at four operating points (Table 2). Two points were located at the design speed line

Table 2 Laser measurements

n, 1/ min	m_{red}, kg/s
50,000	2.83
50,000	2.60
44,000	2.15
35,000	1.40

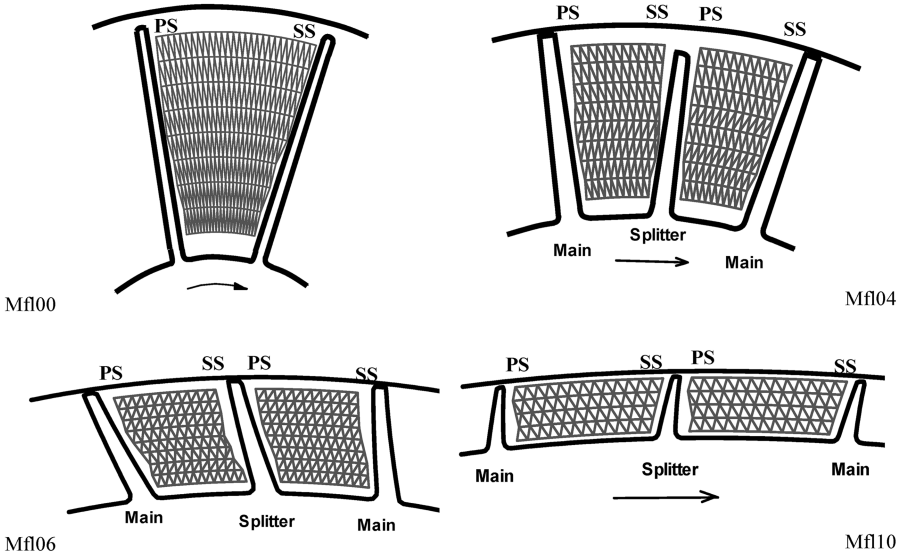

Fig. 9 Grids for laser measurements in planes 00, 04, 06 and 10 indicated in Fig. 8.

($n = 50,000$ 1/ min), and the others were at part load ($n = 44,000$ and $35,000$ 1/ min). At $44,000$ 1/ min, measurements were carried out close to the suction line to find out if any hints about the kink in the suction line could be obtained. For $35,000$ 1/ min, the point of optimum efficiency was chosen for the analysis.

The grids used for the measurements are shown in Fig. 9. In the planes 00, 04, and 06, measurements were carried out at nine channel depths equally spaced from hub to shroud. Because of the rather small channel height at the rotor exit (Mfl10), measurements here were only carried out at five positions. To get information about the flow differences expected left and right of the splitter blade, the flow was analyzed across two blade pitches at 40, 60, and 100% flowpath length. About 12 measurement points were generally available at each depth between the pressure and suction sides.

At each measurement point, the user of the 3C measurement system gets the 3 absolute-velocity components and information about the turbulence intensity. The compressor has no inlet guide vanes and no inlet swirl. Because the local circumferential velocity and the total temperature at the rotor inlet are known, additional flow quantities such as relative velocity, relative Mach number, relative flow angle, etc., can be derived from measurements for the relative system by using the kinematic relations.

The experimental investigations were accompanied by numerical 3-D flow simulations[†] [11] with the flow solver TRACE (Turbomachinery Research Aerodynamics Computational Environment), that is capable of performing steady and unsteady flow calculations for the entire compressor stage [12,13]. TRACE has been validated by a number of test cases for axial and radial compressors.[†]

TRACE is a parallelized, multiprocessable, multiblock Reynolds-averaged Navier–Stokes flow solver for structured and unstructured grids, developed specifically for modeling and investigating turbomachinery flows, including casing treatment, bleeding, aeroelastic simulations, and surface roughness. TRACE has established itself as the standard numerical tool for internal flow computation at DLR, German Aerospace Center. It is also widely used at universities and other research institutes throughout Germany. Additionally, the code is used by the industry for developing and optimizing engine and gas turbine components.

For the centrifugal compressor stage under consideration, TRACE was run in steady flow mode with a mixing-plane approach. Nonreflecting boundary conditions were used at the inlet and outlet of the computational domain.

Figure 10 shows a comparison of relative Mach number distributions derived from the velocity measurements at the rotor inlet for both the new and the old rotors (Figs. 1 and 8, Mfl00). In both cases, the measurement planes are perpendicular to the machine axis and touch the tip of the main blade leading edge. Because the new rotor has backswept leading edges (Fig. 8), these measurements were inside the flow channel. For the old rotor, having radially oriented leading edges, measurements in this plane were carried out just ahead of the leading edge. Because the impellers have identical main dimensions and were designed for the same operating point, the overall velocity and Mach number levels are similar. The maximum relative Mach number is in the range of 1.4. The shock, indicated by the strong gradient in the contour lines, is predicted to be slightly weaker by CFD, due to the coarser mesh spacing used at midpitch. As previously mentioned, the absolute axial position of the visualization planes is different, due to the backward lean of the new rotor leading edge. For the predecessor rotor, a pronounced separated leading-edge flow was found on the suction side. For the new rotor, such a separation does not occur. This agrees with the design philosophy, which especially aimed at an improvement of the flow just at this position [6]. The separation was avoided by introducing a twist and a backsweep of the main blade leading edge.

Similar Mach number distributions are shown for measurement plane Mfl04 in Fig. 11. Inside the new rotor, this plane is located just at the splitter-blade leading edge (Fig. 8). For the old rotor, it is positioned completely inside the bladed area. The Mach number level at this position is already much lower than at the inlet. The flow is subsonic throughout. Compared with the old rotor, a more homogeneous flow has developed in the shroud region. Further downstream, this homogenization becomes even more pronounced, which is illustrated in Fig. 12, showing the Mach number distributions for both rotors at 60% meridional flowpath length. The Mach number level is equal in the middle of the flow channels of both rotors, but the gradient between hub and shroud is much less for the new design. In particular, the wake flow region present in the shroud area of the old rotor has vanished in the new impeller, showing that the wake development along the shroud is positively controlled by the shroud contour of the new rotor. For the new rotor, the 3C-measurement technique was applied (Fig. 2). The third velocity component parallel to the laser beam was found to be maximum in this measurement plane. Close to the blade surfaces, this component rose to up to 30% of the L2F measured velocity component, oriented perpendicularly to the laser beam axis.

The new impeller geometry also positively influenced the rotor discharge flow, as can be seen in Fig. 13. It shows the relative Mach number distributions derived from L2F measurements at the exits of both rotors. The difference in blade shape illustrates again that the two rotor geometries significantly deviate at the rotor discharge. For both designs, this view is almost perpendicular to the mean exit flow direction. The contour line patterns demonstrate the more regular

[†]Private communication with B. Hoffman, 2006.

flow structure at the exit of the new rotor. This especially applies to the circumferential direction, where the contour lines in the new rotor are more parallel to the hub and shroud than in the old one. A pronounced wake area, as can be seen in the left channel of the old rotor in the hub/suction side region, is not detected at the exit of the new impeller.

Overall, a more homogeneous flow is found in the whole exit area of the new rotor. This is indicated more clearly by the absolute flow

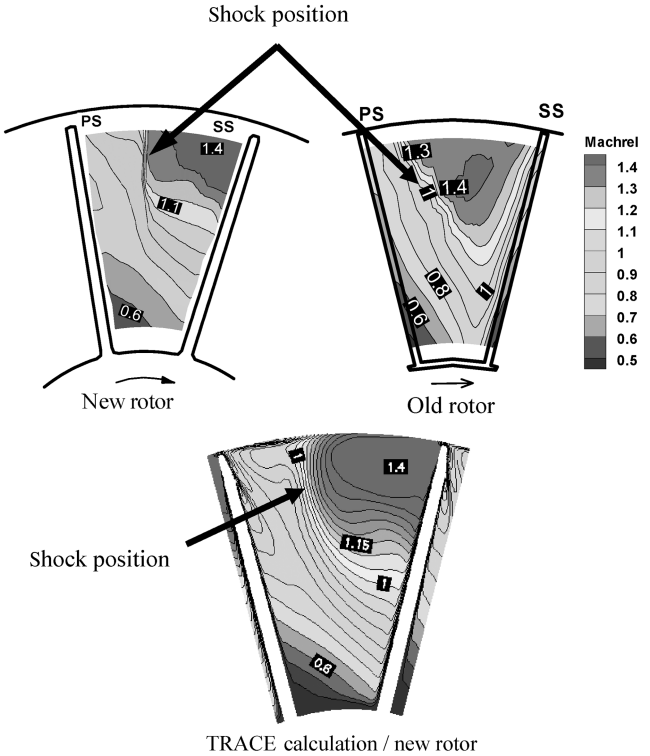

Fig. 10 Relative Mach number distributions derived from laser measurements and calculations at Mfl00 for the old/new impeller; $m = 2.55/2.60$ kg/s and $n = 50,000$ 1/min.

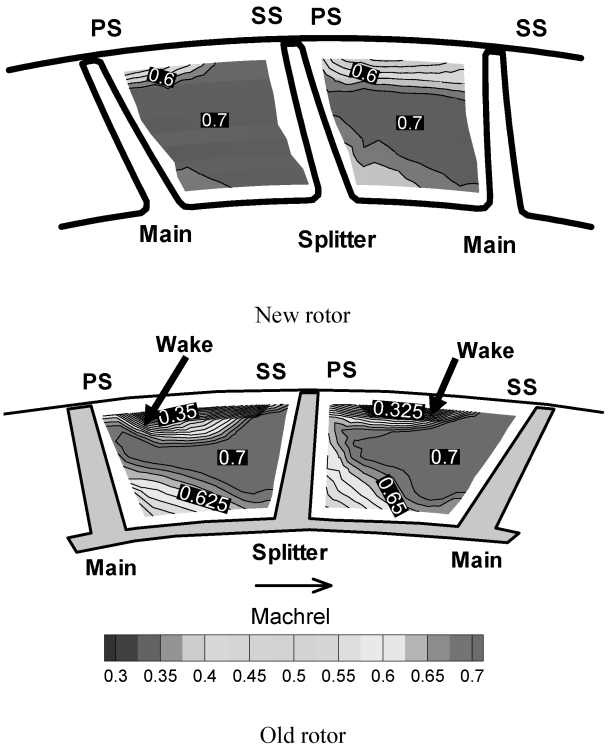

Fig. 12 Relative Mach number distributions derived from laser measurements at Mfl06 for the old/new impeller; $m = 2.55/2.6$ kg/s and $n = 50000$ 1/min.

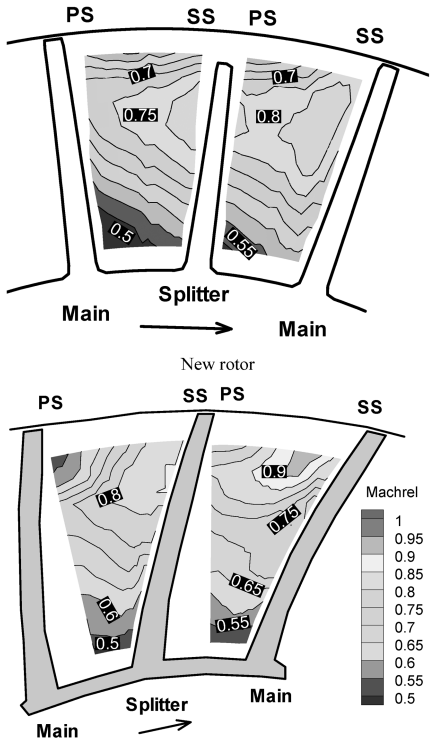

Fig. 11 Relative Mach number distributions derived from laser measurements at Mfl04 for the old/new impeller; $m = 2.55/2.6$ kg/s and $n = 50000$ 1/min.

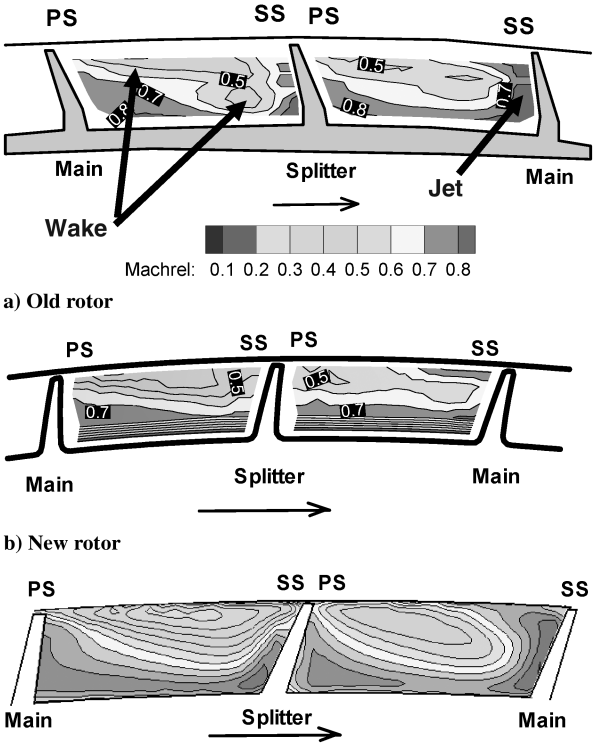

Fig. 13 Relative Mach number distributions derived from measurements and TRACE calculations at Mfl10 for the old/new impeller; $m = 2.55/2.6$ kg/s and $n = 50,000$ 1/min.

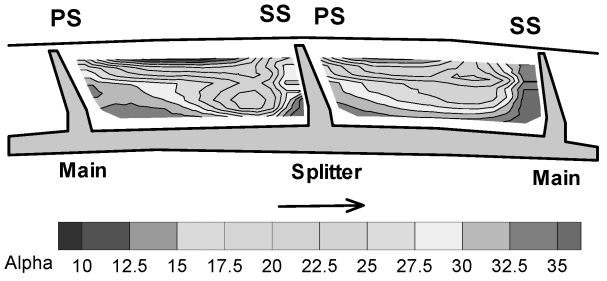

a) Old rotor

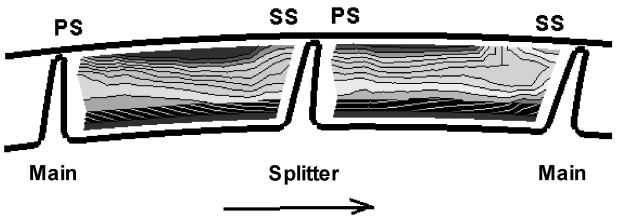

b) New rotor

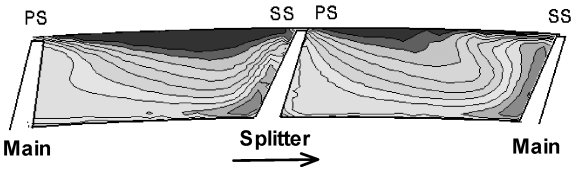

c) New rotor, TRACE calculation

Fig. 14 Absolute flow angle (degrees) distributions derived from measurements and TRACE calculations at Mfl10 for the old/new impeller;$m = 2.55/2.6$ kg/s and $n = 50,000$ 1/min.

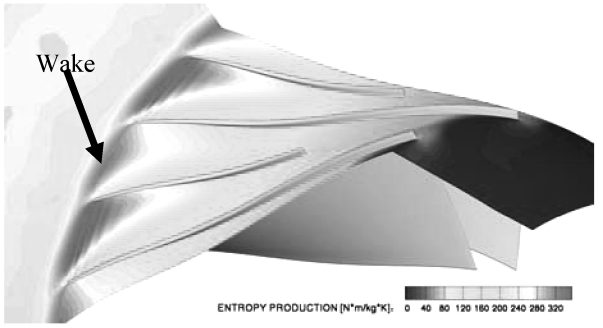

a) Old rotor

b) New rotor

Fig. 15 Entropy production for the old/new impeller derived from 3-D calculations at 93% span from hub; $m = 2.55$ kg/s and $n = 50.000$ 1/min.

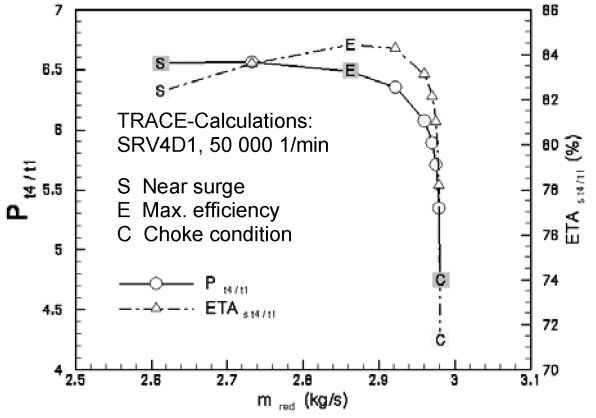

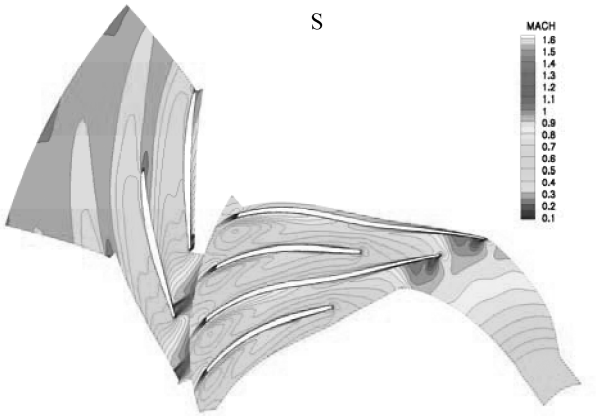

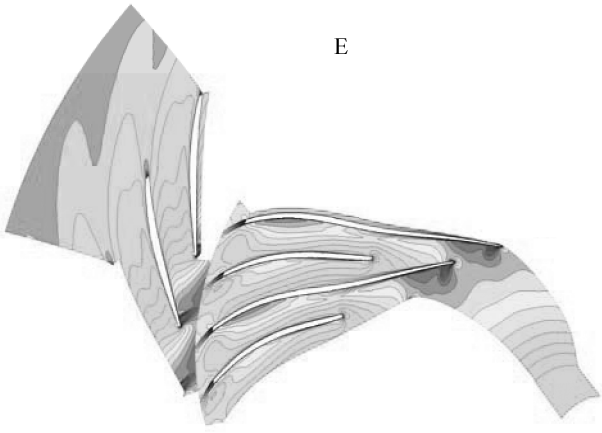

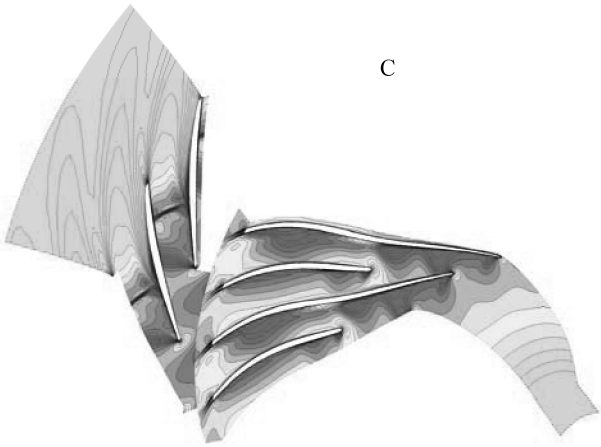

Fig. 16 Calculated Mach number distributions at 60% channel height, design speed $n = 50,000$ 1/min, and different operating points (S, E, and C).

angles at the rotor exit shown in Fig. 14. Because of secondary flow, tip clearance, and jet/wake flow, which mix at the rotor discharge, the flow character in high-pressure-ratio compressors is generally most complex at this position. Considering this, the measured and calculated flow values and the structure of the contour lines are in excellent agreement. No measurement results were available close to the channel surfaces (blades, hub, and casing). Because the CFD calculated and the measured flowfield agree well in the overlapping region, it can be assumed that the simulated near wall field is also close to reality.

From the theoretical calculations it was found that loss production has its maximum in the vicinity of the casing of both impellers. In agreement with the findings of Fig. 14, it is noticeably higher in the old than in the new impeller. This is pointed out in Fig. 15, showing the predicted entropy production for both designs at 93% span. Because of the modified blade shape and meridional contour, entropy production starts much later in the new than in the old impeller, resulting in a significantly lower level and more regular structure in the pitchwise direction at the rotor discharge. The pronounced loss concentration observed in the wake of the old rotor disappeared in the new design. In the core flow, at smaller span positions, the entropy production was found to be on a similar level for both rotors.

Three numerical TRACE solutions for different operating points at design speed are shown in Fig. 16. The operating points chosen are marked on the calculated speed line (S, E, and C). They describe a throttling process from surge (point S) to maximum efficiency (point E) to choke (point C).

Mach number distributions were plotted on blade-to-blade surfaces for 60% channel height from the hub. For the rotor section, the relative Mach number distribution is plotted, and for the diffuser section, the absolute Mach number distribution is plotted. Close to surge (point S), local supersonic flow areas are present at the diffuser inlet as well as at the rotor leading edge. Shocks are observed in the diffuser inlet area, extending into the rotor exit region. As also seen in the measurements, the flow character is rather regular at this operating condition. Distinct separation regions are not seen in the theoretical solutions. With increasing mass flow (point E), the supersonic flow regions increase in the rotor and diffuser inlet regions. Inside the rotor, supersonic flow also appears close to the main and splitter-blade suction sides. At operating point C, both the rotor and diffuser are completely choked. The diffuser flow is significantly accelerated at the diffuser inlet part. The shock has moved into the diffuser, generating a pronounced separation at the diffuser pressure side.

V. Conclusions

This paper describes the development of an improved high-pressure-ratio centrifugal compressor rotor. Performance measurement results and detailed optical measurement results of the new rotor are compared with the results of a predecessor rotor of same type. A 3-component laser velocimeter especially developed for measurements in very compact machines are used for the optical investigations. A significant pressure and efficiency rise are found for the new design. The optical measurements show a more homogeneous/regular flow pattern at the exit of the new rotor. The experimental findings are confirmed by theoretical 3-D stage calculations performed with an advanced 3-D Reynolds-averaged Navier–Stokes flow solver TRACE, especially developed for modeling internal turbomachinery flows.

Acknowledgments

The research work presented was sponsored by the German Ministry of Economy via Arbeitsgemeinschaft Industrieller Forschungsvereinigungen e.V. (AIF) and Forschungsvereinigung Verbrennungskraftmaschinen e.V. (FVV) (Bundesministerium für Wirtschaft und Technologie: AIF-no. 13228 N/1, FVV-no. 798). The authors would like to thank these organizations for their permission to publish this paper.

References

[1] Eisenlohr, G., Krain, H., Richter, F. A., and Tiede, V., "Investigations of the Flow Through a High Pressure Ratio Centrifugal Impeller," American Society of Mechanical Engineers Paper GT-2002-30394.

[2] Krain, H., and Hoffmann, B., "Flow Physics in High Pressure Ratio Centrifugal Compressors," ASME Summer Meeting, Washington, D.C., American Society of Mechanical Engineers Paper FEDSM98-4853, June 1998.

[3] Krain, H., "Unsteady Diffuser Flow of a Transonic Centrifugal Compressor," International Society for Air Breathing Engines Paper 2001-1202.

[4] Krain, H., and Hah, C., "Numerical and Experimental Investigation of the Unsteady Flow Field in a Transonic Centrifugal Compressor," *The International Gas Turbine Congress 2003*, Gasturbine Society of Japan, Tokyo, p. 9.

[5] Colantuoni, S., and Collela, A., "Aerodesign and Performance Analysis of a Radial Transonic Impeller for a 9:1 Pressure Ratio Compressor," American Society of Mechanical Engineers Paper 92-GT-183, 1992.

[6] Kang Shun, "Numerical Investigation of a High Speed Centrifugal Compressor Impeller," ASME Turbo Expo 2005, Reno-Tahoe, NV, American Society of Mechanical Engineers Paper GT2005-68092, June 2005.

[7] Schodl, R., "Measurement Techniques in Aerodynamics," *Laser Methods in Fluid Mechanics*, VKI Lecture Series, von Kármán Inst. for Fluid Dynamics, Rhode-Saint-Genèse, Belgium, 1989.

[8] Schodl, R., Förster, W., Karpinski, G., Krain, H., and Röhle, I., "3-Component Doppler Laser-Two-Focus Velocimetry Applied to a Transonic Centrifugal Compressor," *Laser Techniques for Fluid Mechanics*, Springer, Berlin, July 2000, Paper 7-2.

[9] Lohmberg, A., "Parameterstudie und Optimierung Eines Laufrades zum Erreichen Einer Homogenen Strömung," Sulzer Innotec, TR TB02_0037, p. 123.

[10] CFX-TASCflow, Software Package, Ver. 2.11.1, ANSYS, Inc., Canonsburg, PA, 2001.

[11] Krain, H., Hoffmann, B., Rohne, K.-H., Eisenlohr, G., and Richter, F.-A., "Improved High Pressure Ratio Centrifugal Compressor," American Society of Mechanical Engineers Paper GT2007-27100, 2007.

[12] Nuernberger, D., Eulitz, F., Schmitt, S., and Zachcial, A., "Recent Progress in the Numerical Simulation of Unsteady Viscous Multistage Turbomachinery Flows," International Society for Air Breathing Engines Paper 200181, 2001.

[13] Hong, Y., Nuernberger, D., and Kersken, H.-P., "Towards Excellence in Turbomachinery CFD: A Hybrid Structured-Unstructured RANS Solver," American Society of Mechanical Engineers Paper GT2005-68735, 2005.

A. Prasad
Associate Editor